Wear 390–391 (2017) 198–208

Contents lists available at ScienceDirect

Wear

journal homepage: www.elsevier.com/locate/wear

Characterization of damage and triboparticles resulting from fretting of Incoloy 800 steam generator tubes against different materials

S.R. Soria[a,b,*], A. Tolley[a,b], A. Yawny[a,b]

[a] División Física de Metales, Centro Atómico Bariloche, Instituto Balseiro, CNEA, Av. E. Bustillo 9500, 8400 S.C. de Bariloche, Argentina
[b] CONICET (Consejo Nacional de Investigaciones Científicas y Técnicas), Argentina

ARTICLE INFO

Keywords:
Incoloy 800
Steam generator tubes
Triboparticles
Fretting

ABSTRACT

Fretting experiments of Incoloy 800 steam generator tubes against AISI 304, AISI 1060 and Cu (99.9%) cylindrical pads were carried out to evaluate the influence of pad composition on wear damage and on the nature of the triboparticles originated in the process. Tests were performed up to 10^6 cycles in air under an imposed relative displacement amplitude of 75 ± 5 μm and a normal contact load of 40 ± 5 N. Surface damage was characterized using light microscopy, scanning electron microscopy and optical profilometry. The triboparticles detached during the tests were analyzed by transmission electron microscopy and energy dispersive X-ray spectroscopy. Debris particles were agglomerates of nano-crystalline oxide grains sized between 5 nm and 20 nm of the following phases: NiO, $(Fe,Cr)_2O_3$ and $(Ni,Fe)(Fe,Cr)_2O_4$ in the case of the AISI 304 pad, $(Cu,Ni)(Fe,Cr)_2O$ for the Cu pad and $(Fe,Cr)_2O_3$ in the case of the AISI 1060 pad. A preponderance of adhesive wear was found for the Cu and AISI 1060 pads while abrasive wear was predominant in the case of the AISI 304 pad. Tube-pad differential hardness was found to have a minor influence on wear rate compared to the acting main wear mechanism.

1. Introduction

In Pressurized Light and Heavy Water nuclear Reactors (PWR and PHWR), the heat generated in the reactor core is transported by the primary water coolant circuit and interchanged in the Steam Generator (SG) to the water steam secondary system. SGs are large heat exchangers consisting of few thousand steam generator tubes (SGTs) that form the boundary separating the water from the primary and secondary circuits. Hence, SGs are one of the most important components of nuclear power plants and assuring their structural integrity is essential for both the safe and efficient operation of a nuclear power plant.

Wear and fretting damage of SGTs is one of the most important degradation mechanisms in nuclear power plants [1]. Fretting is a damage mechanism originated in the area of contact between two bodies where a persisting oscillating relative movement of small amplitude (1–300 μm) takes place. It is usually caused by flow induced vibrations (FIVs) due to high flow rates and small clearances between the tubes and their supports [2]. Fretting is a complex phenomenon involving different mechanisms such as abrasion, adhesion and tribochemical reactions, among others [3]. In fact, it has been reported that more than 50 factors might influence the process [4], the most significant of which are the normal contact load between the bodies involved and the amplitude of their relative displacement. Other factors considered important in determining the damage development are the surface hardness [5,6] and the specific chemical composition [7,8] of the materials in contact. At the same time, the triboparticles (debris) formed during the process itself influence the subsequent damage. This relationship between the generated triboparticles and the resulting fretting damage has been studied elsewhere [9–12] for some steels and Ni based alloys.

Alloy 800, alternatively Incoloy 800 (I 800 in what follows), is a material often used in the fabrication of SGTs due to adequate resistance to stress corrosion cracking and mechanical behaviour at temperatures around 300 °C [13], typical of primary water circuits in PWR and PHWR. Studies about fretting damage on I 800 have been performed under different environmental conditions and contact configurations, for example, tube-plate and tube-tube configurations [14,15]. These studies showed that temperature influences the wear rate in a complicated way [14] and that differences in the wear rate depend on the chemistry of the materials in contact [15]. Despite these studies, a detailed understanding of the mechanisms involved in the complex fretting process in I 800 is still lacking. In a recent work [16], the fretting wear behaviour in air at room temperature of I 800 SGTs against AISI 304 solid pads was studied for displacement amplitudes of

* Corresponding author at: División Física de Metales, Centro Atómico Bariloche, Instituto Balseiro, CNEA, Av. E. Bustillo 9500, 8400 S.C. de Bariloche, Argentina.
E-mail address: sergiorsoria@gmail.com (S.R. Soria).

http://dx.doi.org/10.1016/j.wear.2017.07.022
Received 22 March 2017; Received in revised form 29 July 2017; Accepted 29 July 2017
Available online 02 August 2017

Table 1
Chemical composition (wt%). of the different materials used in the present work.

Material	Fe	Ni	Cr	Cu	C	Mn	S	Si
I 800	42.2	33	21.6	0.09	0.017	0.55	0.003	0.54
AISI 304	66.6 min	8–11	18–20	–	0.08	2	0.003	1
AISI 1060	98 min	–	–	–	0.55–0.65	0.6–0.9	0.05 max.	0.15–0.35
Cu	–	–	–	99.9	–	–	–	–

70, 116 and 160 μm and a nominal normal load of 35 N up to 10^6 cycles. Gross slip regime was found in all cases with the formation of different surface layers depending on the displacement amplitude. In addition, the detached debris were characterized by TEM indicating a wide dispersion in the particle sizes in all tests, ranging between 100 nm and 500 nm. It was shown that the debris were constituted by agglomerates of nanocrystalline particles with individual sizes between 5 nm and 20 nm consisting of non-stoichiometric oxides originated by tribochemical reactions in the contact area. Further details about the characteristics of the surface layer and the nature of the triboparticles were also reported [16].

As a next step in contributing to a better understanding of the role of the different variables that affect the complex fretting process, the influence the pad composition on the mechanisms of fretting wear damage was addressed in the present work. To this purpose, experiments have been performed on I 800 SGTs against pads of AISI 304 stainless steel, AISI 1060 medium carbon steel and 99.9% purity Cu. Partial results of these studies have been published in the proceedings of the Congress SAM-CONAMET 2014 [17]. The main reasons behind the different pad´s materials adopted are briefly explained in what follows. AISI 304 is often considered as alternative candidate for different components that might fret against I 800 SGT, thus its importance. Cu represents a radically different composition with respect to the one of I 800 and enables exploring how such difference impacts on the resulting fretting behaviour. AISI 1060 was chosen to examine, by comparing with AISI 304, the influence of Cr, Ni on the fretting behaviour. For each pair combination, the nature of the wear mechanisms (adhesive or abrasive), its relationship with the structure of the corresponding debris and the respective Archard-based wear coefficient were determined.

2. Materials and methods

SGTs of I 800 with 15.87 mm diameter and 1.13 mm wall thickness provided by FAE S.A. (Argentina) were employed in the present study. The pads were fabricated using AISI Type 304 stainless steel, AISI 1060 carbon steel and 99.9% purity Cu with solid semi-cylinder geometry and a diameter of 13.5 mm. The detailed nominal composition of the materials used is presented in Table 1. Vickers Hardness (HV) of the external surfaces of I 800 tube and pads were determined using a Mitutoyo MKV-H0 hardness tester using a load of 0.3 kgf. The results are presented in Table 2

The fretting test rig consisted in an elastic cantilever beam mounted in a MTS 810 servo-hydraulic testing machine as shown in Fig. 1 (details have been published elsewhere [16]). The SGT tube was gripped in the vertical direction to the mobile piston using the bottom hydraulic grip shown in the figure while the pad counterpart was fixed in a 90° cross cylinder configuration to the cantilever beam at a precalibrated distance, according to the desired normal contact load. The direction of the imposed relative displacement was coincident with the longitudinal direction of the SGTs and transversal to the longitudinal direction of the semi cylindrical pads. The normal load applied in the experiments was $F = 40\ \text{N} \pm 5\ \text{N}$. The error of F included the combined effect of the uncertainty in positioning the pad along the elastic beam and the load change that might occur during the test due to the small variation in beam deflection associated with the development of the scar. The imposed relative displacement was sinusoidal with a frequency 15 Hz and a displacement amplitude of $\delta = 75 \pm 5$ μm. Tests were conducted in air at room temperature (25 °C, 35% relative humidity) up to a total of $N = 10^6$ cycles. Although this does not correspond to actual operating conditions (i.e., aqueous environment, 300 °C), using the room temperature dry air environment is a convenient a first step in tackling the problem.

Surface damage on SGTs and pads after testing was characterized using a Leica DMR Light Microscope (LM) and a Phillips 515 Scanning Electron Microscope (SEM). The specimens were cleaned using an ultrasonic bath with acetone and ethanol in order to remove debris and loosely adhered surface layers. The depth of the scar was then determined with a Wyko NTC1100 optical profiler. Energy Dispersive X-ray Spectroscopy (EDS) elemental mapping and line composition analysis was performed in a FEI Nova Nano SEM 230.

Debris detached during testing were characterized using a Philips CM200 Transmission Electron Microscope (TEM) operated at 200 kV, equipped with a LaB_6 cathode, an Ultratwin lens and an EDAX EDS microanalyser. For this purpose, debris were collected in a clean paper cup throughout the test. A colloidal suspension was obtained by adding the collected debris into ethanol. A Cu grid with Formvar/Carbon film was then immersed in the suspension. Particles that remained attached to the film were studied by TEM.

Table 2
Vickers Hardness (HV) of the external surface of the I 800 SGT and the different pad materials used in the present work.

Material	I 800	AISI 304	AISI 1060	Cu
HV [kgf/mm^2]	215 ± 22	321 ± 23	753 ± 43	143 ± 7

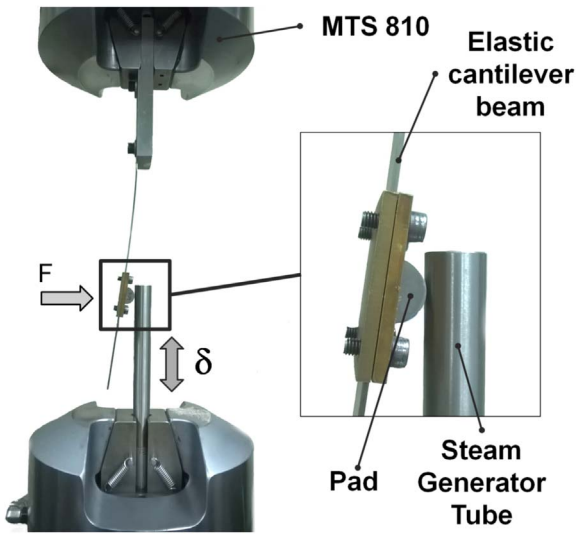

Fig. 1. Fretting wear test rig used [16].

3. Results and discussion

3.1. Analysis of surface damage

The characteristic features of the wear scars on SGTs and pads after ultrasonic cleaning are shown in the LM images presented in Fig. 2 and the SEM images in Fig. 3. The black arrows indicate the displacement direction. The scars present a circular shape, typical of the 90° cross cylinder geometry used in the tests. In all cases, sliding marks aligned in the direction of the relative displacement were observed (Fig. 3), suggesting that gross slip is the dominant fretting running condition in all the experiments performed.

The SEM micrographs of the scars corresponding to the I 800/AISI 1060 and I 800/Cu pairs show the formation of a layer of compacted-debris on the surface of the pad and the SGTs (Fig. 3(b) and (c)). For the I 800/AISI 1060 pair the compacted debris layer is more evident on the SGT scar, Fig. 3(b), where it presents a brighter appearance. In the pad, the compacted debris layer was considerably smaller than that observed in tube scar. For the I 800/Cu combination, the formation of a bright compacted debris layer was observed in both tube and pad, as shown in Fig. 3(c). In this case, delamination of the debris layer in the pad scar can also be observed. On the other hand, in the I 800/AISI 304 pair, grooves due to third body abrasion constitutes the predominant feature as can be observed in Fig. 3(a), suggesting that abrasion is the main wear mechanism in this case. Additional experiments under the same normal load but performed using a displacement amplitude of 40 μm resulted in the same main wear mechanisms (results not included here for the sake of brevity).

Gross slip conditions were identified in all the SGT/pad combinations. In these conditions, the principal damage mechanism is wear and removal of material from the contact area, as described in [18].

To evaluate the effects of the pad´s composition on the wear process, the total volume of material removed, V, was determined. In the present work, this volume is defined as the sum of the volumes V_{SGT} and V_{PAD} of material removed from the SGT and the corresponding pad, respectively. An optical profiler was used to measure maximum radial depth profile of the SGTs´ and pads´s scars. From these profiles the removed volumes, V_{SGT} and V_{PAD}, and the maximum scar depths, h_{SGT}

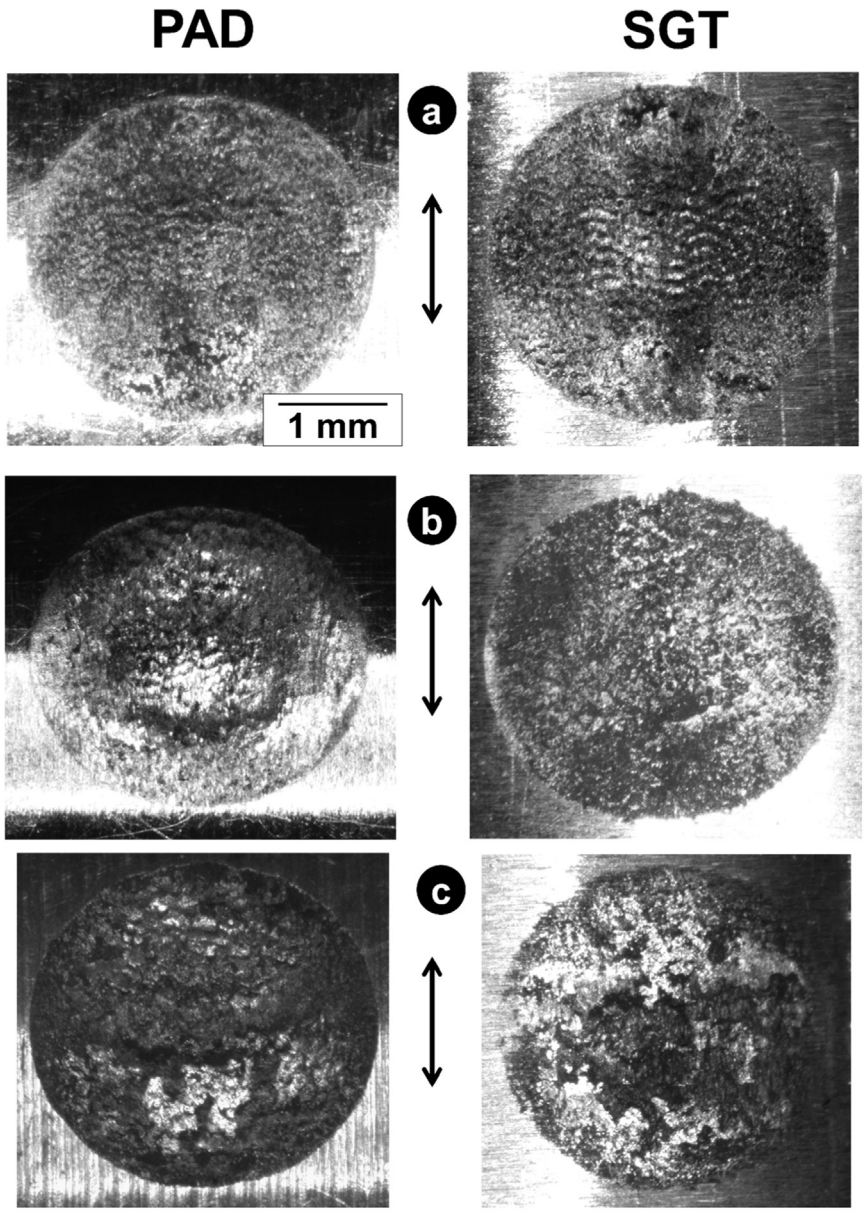

Fig. 2. LM images of fretting scars produced in pads and I 800 SGTs for different pad´s materials: (a) AISI 304, (b) AISI 1060 and (c) Cu. Arrows indicate the relative displacement direction.

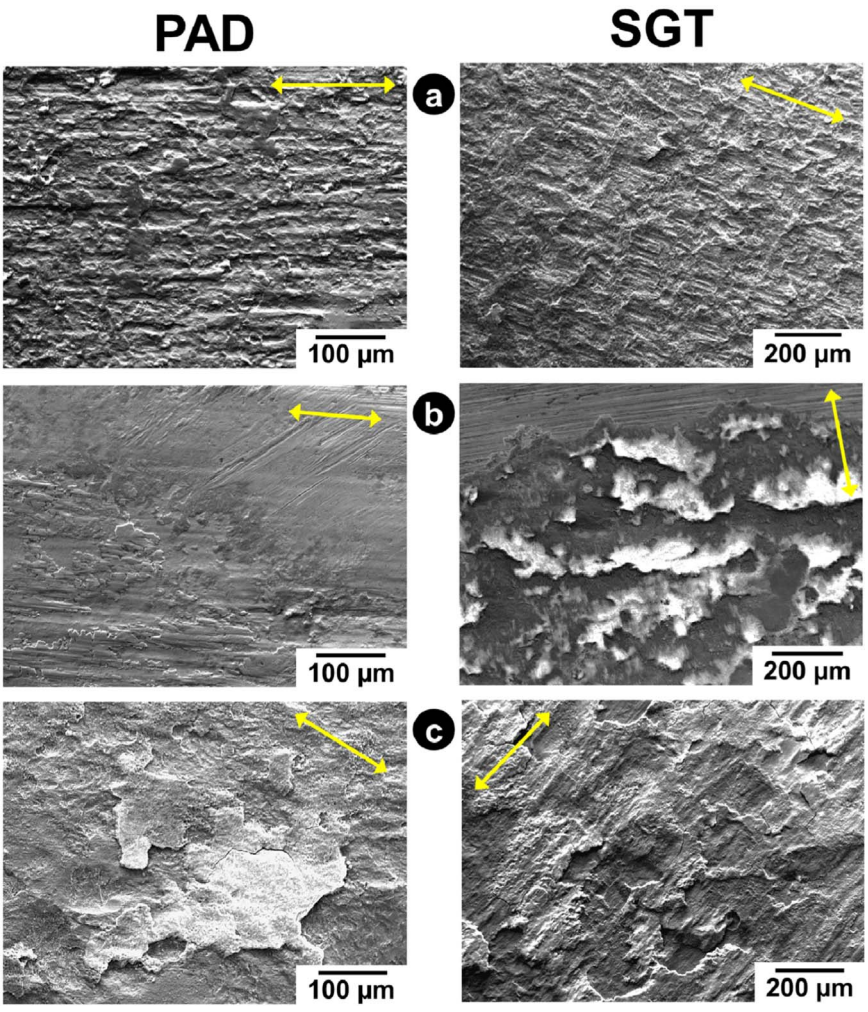

Fig. 3. SEM images of fretting scars produced in I 800 SGTs and pads of different materials: (a) AISI 304, (b) AISI 1060 and (c) Cu. Arrows indicate the displacement direction.

and h_{PAD}, were determined. It is important to remark that proceeding in this way, the volume V was measured and not indirectly estimated using the equations recommended by ASTM G-204 standard test [19]. This is an important issue since in reference [16] it was shown that the ASTM method strongly overestimates the removed volume.

From V, the fretting Archard-based wear coefficient K (in Pa^{-1}) was calculated using Eq. (1) [20]:

$$V = K \cdot F \cdot S \Rightarrow K = \frac{V}{F \cdot S} = \frac{V}{F \cdot 4 \cdot \delta \cdot N} \quad (1)$$

Here, F is the applied normal load and S is the total displacement distance calculated from the displacement amplitude δ and the number of cycles N ($4 \cdot \delta$ is the total displacement distance per cycle).

The results are presented in Table 3 and Fig. 4.

From Fig. 4(b) and (c) it can be seen that for the I 800/AISI 1060 and I 800/Cu pairs the centre of the pads´ scars are much deeper than the corresponding scars on the SGTs. Instead, in the case of the I 800/AISI 304 pair, Fig. 4(a), the depth profiles of the scars in both SGT and pad are very similar. In addition, it can be seen that h_{SGT} is greater that h_{PAD} whereas V_{SGT} is smaller than V_{PAD}. This indicates that there is not a direct correlation between the scar depth and the corresponding removed volume. This is a consequence of the shape of the wear scar as shown in Fig. 4.

Table 3
Wear volume removed V and maximum scar depth h in SGT and PAD and Archard-based wear coefficients K for the different SGT/pad´s combinations.

Pad	AISI 304	AISI 1060	Cu
h_{SGT} [µm]	105	42	20
V_{SGT} [mm^3]	0.51	0.34	0.08
h_{PAD} [µm]	92	112	155
V_{PAD} [mm^3]	0.62	0.59	0.90
V [mm^3]	1.13	0.93	0.98
K [Pa^{-1}]	9.4×10^{-14}	7.8×10^{-14}	8.2×10^{-14}

In the depth profile of the SGT scar of the I 800/Cu pair shown in Fig. 4(c), some regions within the scar area are in fact higher than the original undamaged surface. In order to explain this effect the occurrence of material transfer between pads and SGTs was considered. For this purpose EDS elemental mapping and EDS elemental line profile analysis were performed in the I 800/AISI 1060 and the I 800/Cu pairs. In both cases a high adherence of detached debris on the metals surface was observed. For the I 800/AISI 1060 pair the elements Ni and Cr were selected to trace material transfer to the pad, since they are only present in the SGT. Instead, for the SGT an increase in the Fe content was used as an indicator of material transfer from the pad to the SGT. For the I 800/Cu pair, the Cu content was used to analyse material transfer from the pad to the SGT.

Fig. 5 shows the results of EDS elemental mapping of the AISI 1060 pad in the region near to the edge of the scar that includes a zone outside the scar, indicated as N.D., no-damage region. Ni and Cr were only detected within the scar zone, with a higher concentration in the attached debris layer. The distribution of Fe was homogeneous both in the scar and in the N.D. region, except in the attached debris layer, where the Fe content was lower. Oxygen was only found within the scar, but not in the No-damage region, indicating that the wear process

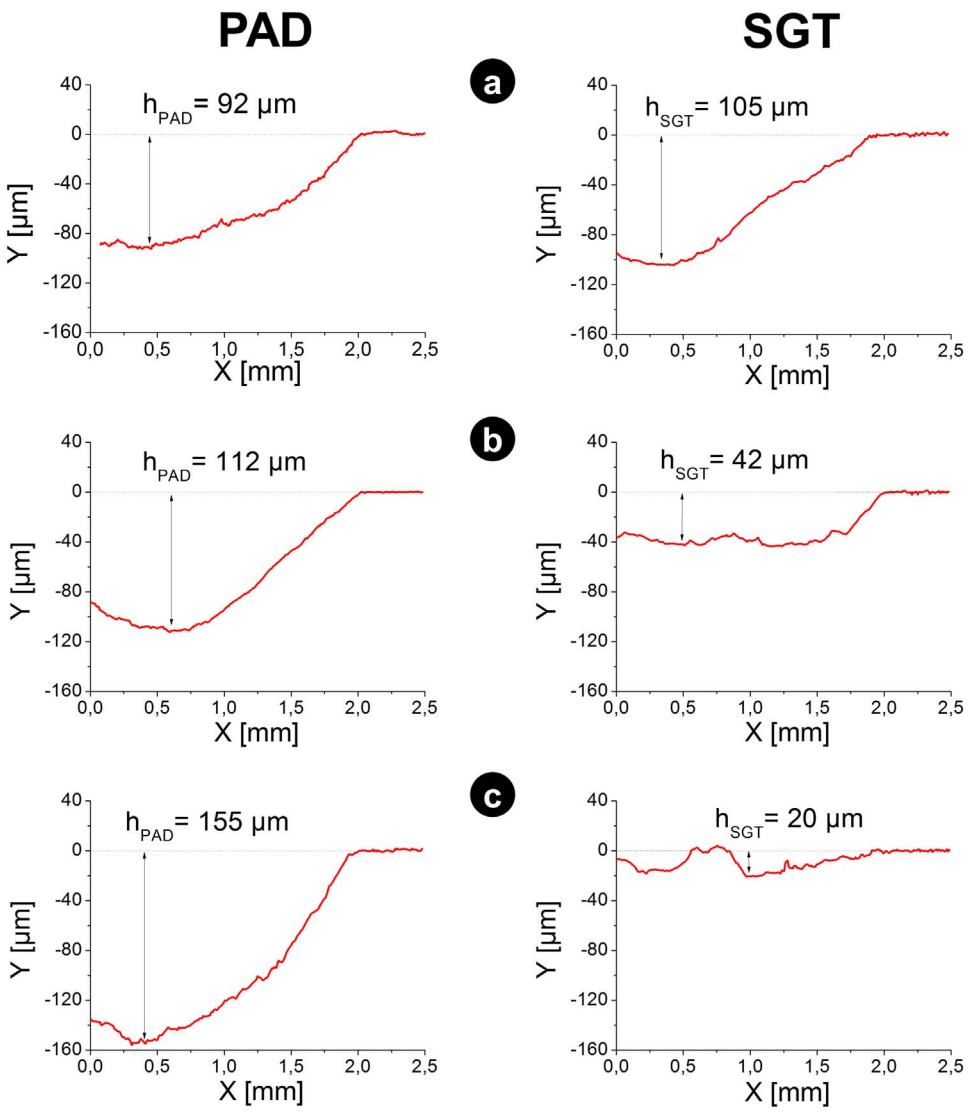

Fig. 4. Central profile of scars on the pads and SGTs for pad of (a) AISI 304, (b) AISI 1060 and (c) Cu.

stimulates the formation of oxides on the worn surface. These results show that material worn from the pad is attached to the SGT, and therefore indicates that material is effectively being transferred from the pad to the SGT. Material transfer therefore explains the marked asymmetry between the depth profiles of the SGTs and pads shown in Fig. 4(b) and (c).

Fig. 6 presents EDS line profile analysis performed in the SGT scar of the I 800/AISI 1060 pair along two lines indicated as A and B, each crossing a compacted debris layer. The arrows indicate the position on the SEM image. In both lines, an increase in Fe content was detected together with a decrease of Ni and Cr in the compacted debris layer. This increase in Fe concentration indicates material transfer from the pad to the SGT.

EDS elemental mapping in the Cu pad scar of the I 800/Cu pair shows that the content of Fe, Ni and Cr was very low (Fig. 7), indicating very little material transfer from the SGT to the pad. This result is consistent with the depth profile on the Cu pad shown in Fig. 4(c). A homogeneous distribution of O was observed on the worn surface. This indicates enhanced oxidation of the original Cu metal surfaces within the fretting scars.

Fig. 8 shows the results of EDS line profile analysis within the SGT scar in the I 800/Cu pair along lines that cross over compacted debris layers. The content of Fe, Ni and Cr decreases in the compacted debris layer, while the Cu content increases above 50%. These results again indicate material transfer from the pad to the SGT.

Fig. 9 presents a SEM image of the SGT scar for the I 800/Cu pair that shows the formation of 3 spherical shaped debris particles with an average diameter of 4 µm adhered to the compacted debris layer. In addition, spherical indents of the same size as the spherical debris particles can be observed.

The presence of spherical particles in sliding wear has been previously observed. It was proposed that they are formed when adhesive wear particles are trapped within cavities in sliding surfaces, where they become smoothed by sliding and rolling within the cavity [21]. Hurricks [22] had previously reported spherical debris in fretting tests of steels in inert atmosphere (Ar gas). The presence of spherical debris particles observed in the present work further supports that adhesive wear is the main wear mechanism in the case of the I 800/Cu pair.

The central profiles of the scars presented in Fig. 4 suggest that different damage mechanisms are prevalent, depending on the pad composition. For the I 800/AISI 304 pair, the main wear mechanism was abrasive wear with the formation of grooves in the displacement direction and a negligible amount of material adhered on the worn surface. Instead, for the I 800/AISI 1060 and I 800/Cu pairs the main wear mechanisms was adhesive wear with the development of a significant compacted debris layer, strongly adhered on the surface. These layers explain the shallower depth of central profile on the SGT compared to that of the corresponding pad. Moreover, the predominance of

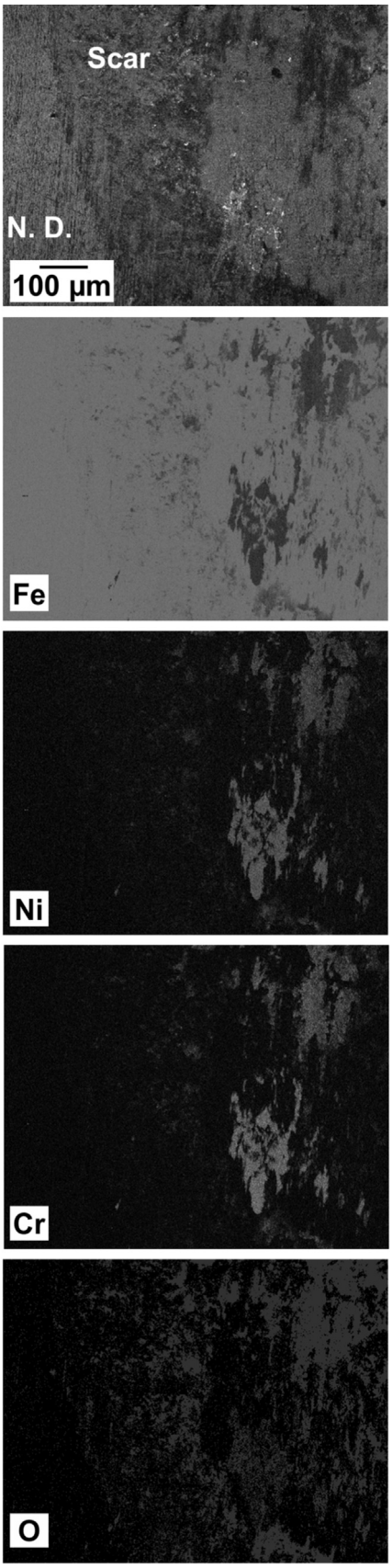

Fig. 5. EDS elemental mapping of Fe, Ni, Cr and O (bright: high concentration, dark: low concentration) performed on pad scar area for I 800/AISI 1060 pair.

adhesive wear is supported by the presence of spherical debris in the worn surface of the SGT scar, shown in Fig. 9.

3.2. Differences in wear coefficient K for the studied material pairs

The wear coefficients of the different pairs studied are presented in Table 3. Measured values for the particular pairs differ less than 20%, with an average of 8.4×10^{-14} Pa^{-1} (equivalent to 8.4×10^{-5} $mm^3/N.m$). The value obtained for I 800/AISI 304 is about 6% smaller than that reported in reference [16] where the total volume removed, V, was estimated as twice the volume removed from the pad, V_{PAD}. From the results presented in Table 3, it can be seen that V_{SGT} is slightly smaller than V_{PAD}. Therefore, $2V_{PAD}$ overestimates the total volume of material removed, which explains the larger value for the wear coefficient reported in reference [16]. It may be noted in passing, however, that $h_{SGT} > h_{PAD}$, contrary to what would be expected from the fact that $V_{PAD} > V_{SGT}$. This is related with the peculiar shape of the wear scars denoted by the central scar profiles shown in Fig. 4.

Reported values of the wear coefficient for the I 800/AISI 410 pair at room temperature and different contact conditions present a high dispersion, ranging from 1.1×10^{-14} Pa^{-1} [14] to 6.7×10^{-14} Pa^{-1} [15]. The wear coefficients obtained in the present study are of the same order of magnitude, somewhat higher than those reported in the literature. Moreover, EDS-elemental mapping and EDS line analysis demonstrated that an important fraction of material removed is deposited and adhered on SGT´s surface. If the adhered material were to be excluded, the volume of material removed and the K value calculated from it would be even larger and so would be the difference with respect to previously published values.

The role of hardness on fretting wear behaviour is not completely clear so far. Recent studies about fretting in hardened steels suggest that a slight hardness differential can reduce the damage and that a lower hardness increases the wear volume [6]. However, other studies have shown that not only the hardness or differential hardness of the pair are important for fretting wear behaviour but the elemental compositional of materials in the pair and the microstructure of debris formed during fretting process [23,24] must also be taken into account.

Fig. 10 shows a plot of the wear coefficient K and the maximum depth of central profile of the pad´s scars, h_{PAD}, versus the Vickers hardness of different pads. No simple dependence of either K or h_{PAD} with hardness can be observed. The lowest value of K was obtained for the AISI 1060 pad, that has the highest hardness and highest differential hardness with respect to the SGT. This result is in agreement with the conclusions of Budinski [6]. However, the wear coefficient for the Cu pad measured in the present work is very similar to that of the AISI 1060 pad, even when Cu has a much lower hardness and differential hardness with respect to the SGT. For both Cu and AISI 1060 pads, adhesive wear was identified as the main wear mechanism. The maximum measured wear coefficient corresponded to the AISI 304 pad, for which abrasive wear was the main mechanism.

The previous results indicate that hardness is not the only parameter controlling the wear process, but that the adhesion of a compacted debris layer, and therefore the wear mechanism, also play a significant role. The maximum scar depth of the pad also presents a complex dependence on the different parameters involved in the process. Again, no simple trend with hardness is observed in Fig. 10. In addition, while the wear coefficients for the Cu and the AISI 1060 pads are similar, the maximum depths differ considerably. Furthermore, the AISI 304 pad presents the maximum wear coefficient but also the minimum h_{PAD}. It is clear that there is no simple correlation between K hand h_{PAD}. Finally, regarding h_{SGT}, the maximum depth was measured for the I 800/AISI 304 pad, where the wear mechanism was abrasive, whereas for the I 800/AISI 1060 and I 800/Cu pairs h_{SGT} was much smaller, due to the preponderant adhesive wear mechanisms in the latter.

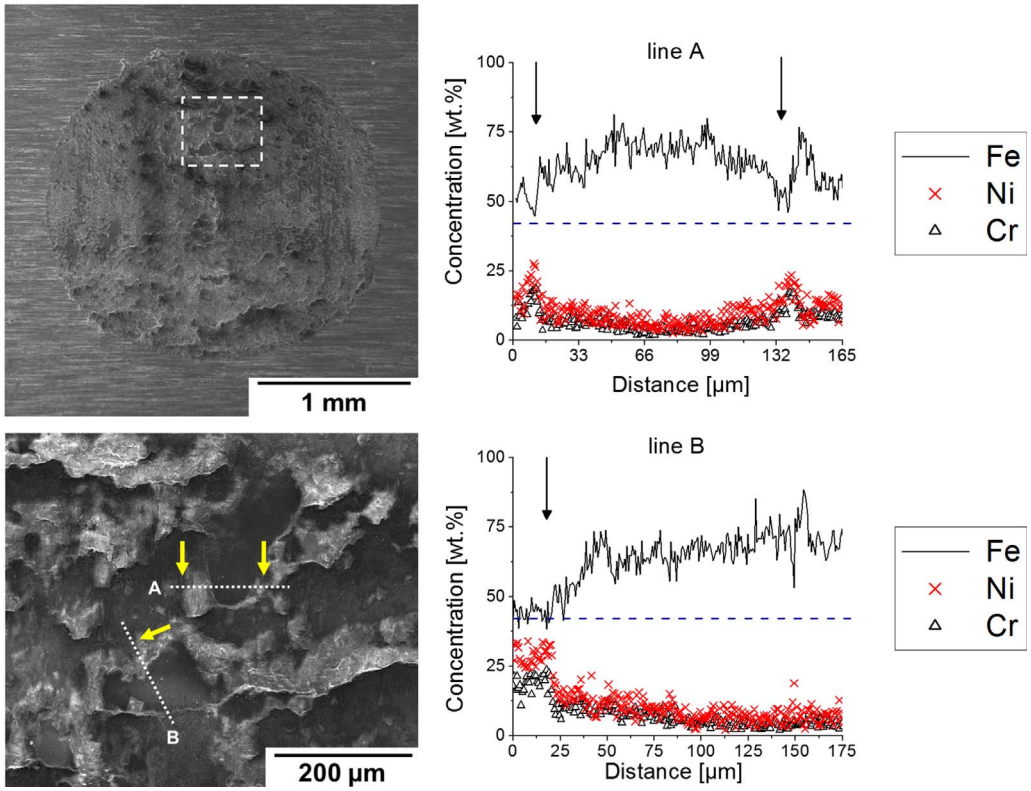

Fig. 6. EDS elemental line scan analyses of Fe, Ni and Cr on SGT for I 800/AISI 1060 pair. Arrows indicate the position in the line. The nominal Fe concentration of the SGT is indicated by horizontal dashed lines.

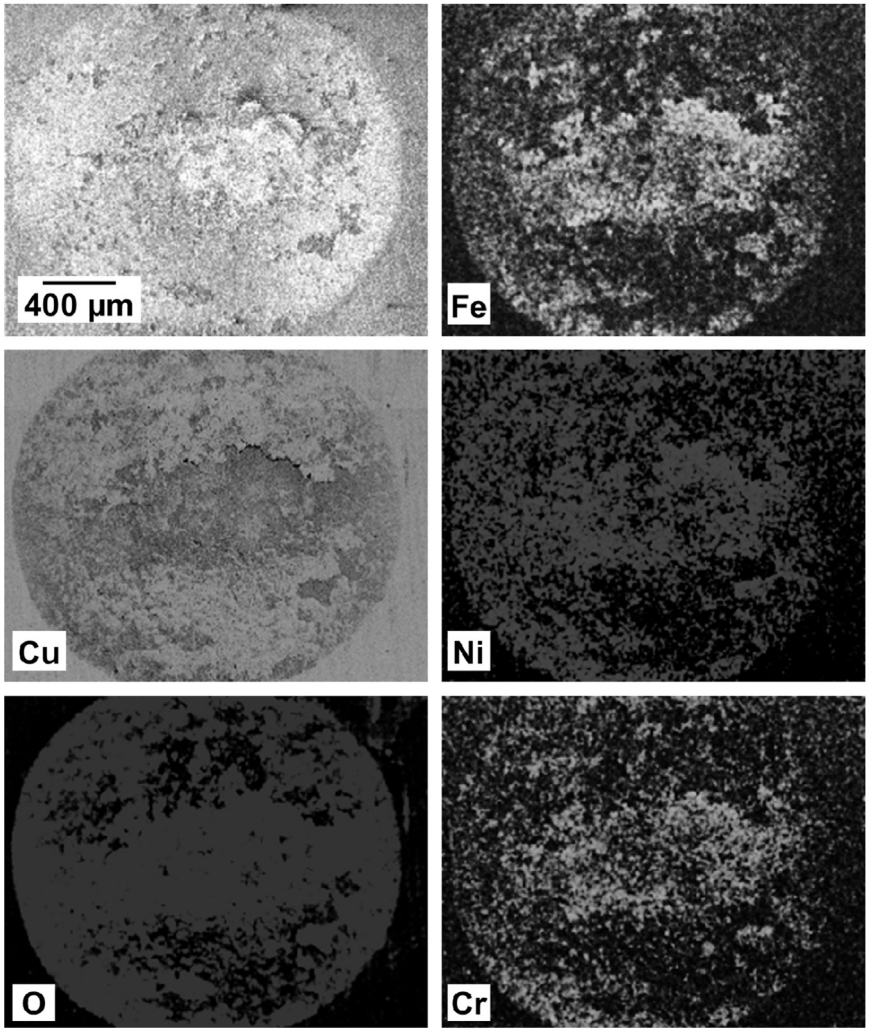

Fig. 7. Scar image (top left) and EDS elemental mappings of Fe, Cu, Ni, O and Cr (bright: high concentration, dark: low concentration) on the Cu pad for the I 800/Cu pair.

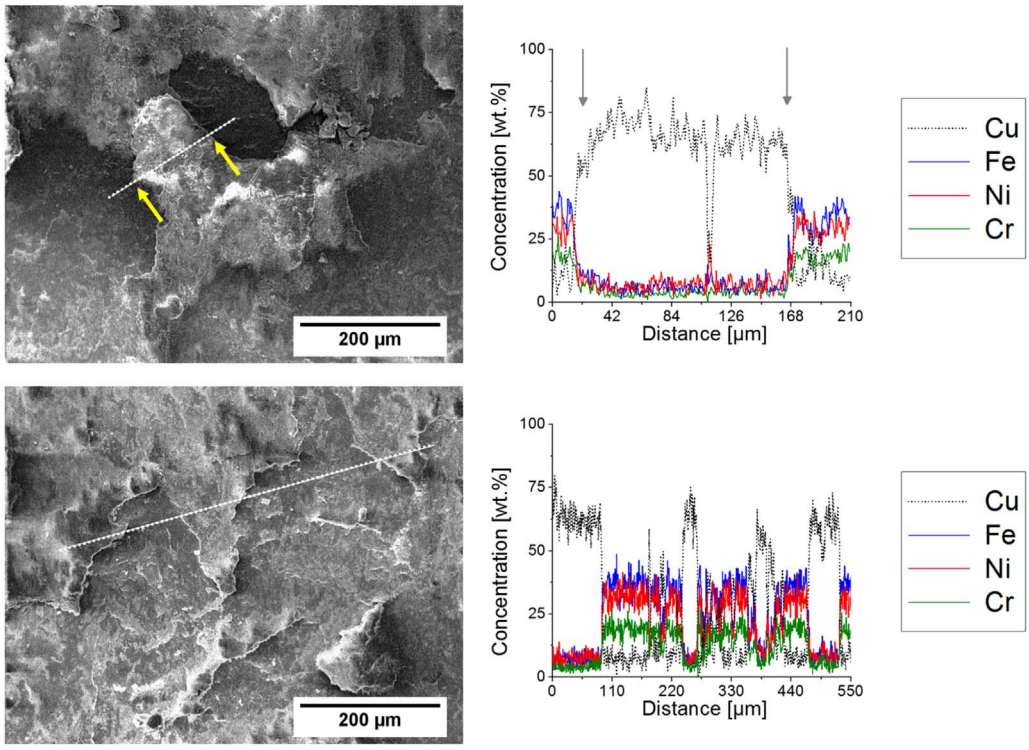

Fig. 8. EDS elemental line scan analyses of Fe, Ni, Cr and Cu on SGT for the I 800/Cu pair. Arrows indicate the position on the line.

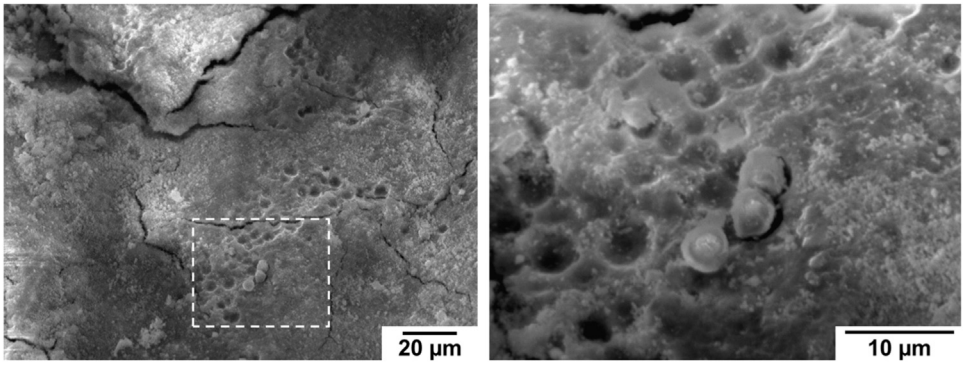

Fig. 9. Evidence of formation of spherical particles on SGT´s scars for I 800/Cu pair.

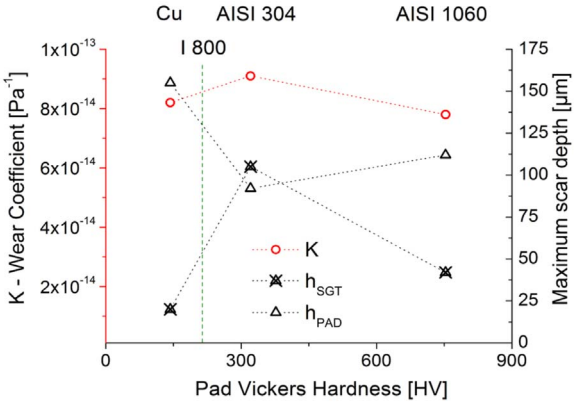

Fig. 10. Evolution of wear coefficient K and maximum depth profile on pad h_{PAD} and SGT h_{SGT} vs. Vickers hardness of pad.

3.3. Analysis of detached triboparticles

Characterization by transmission electron microscopy of the detached debris from the three pairs of materials studied showed that they consisted of particles with a wide size distribution between 100 nm and 500 nm. In Fig. 11, images of the particles obtained for each pair are presented. The particles consisted of an agglomeration of small crystallites with sizes ranging 5–20 nm. The individual nanoparticles presented crystalline contrast under High Resolution TEM (HRTEM) as can be seen in Fig. 12 that corresponds to the I 800/AISI 304 pair.

The crystalline structure of debris detached from the different pairs studied was analyzed using electron diffraction patterns from particles with sizes around a few hundreds of nanometers. The diffraction patterns, shown in Fig. 13, consist of concentric rings of reflections that is consistent with the observation that the particles contain a collection of randomly oriented small crystallites or grains. The local composition within debris particles was studied with EDS spectroscopy as shown in Fig. 11. For the I 800/AISI 304 pair Fe, Cr and Ni were detected in all regions. The peak intensity was found to vary from region to region, indicating that debris have an inhomogeneous composition. Similar effects had been observed for others pair. For the I 800/Cu pair two EDS spectra are presented in Fig. 11(c), one obtained on the debris and the other with the beam impacting on the support grid. Since the grid consists of Cu wires supporting a formvar/ carbon film, the spectrum from the latter contains intense Cu K and C K peaks and a very weak Cu L peak due to absorption within the thick Cu wires. Instead, in the spectrum

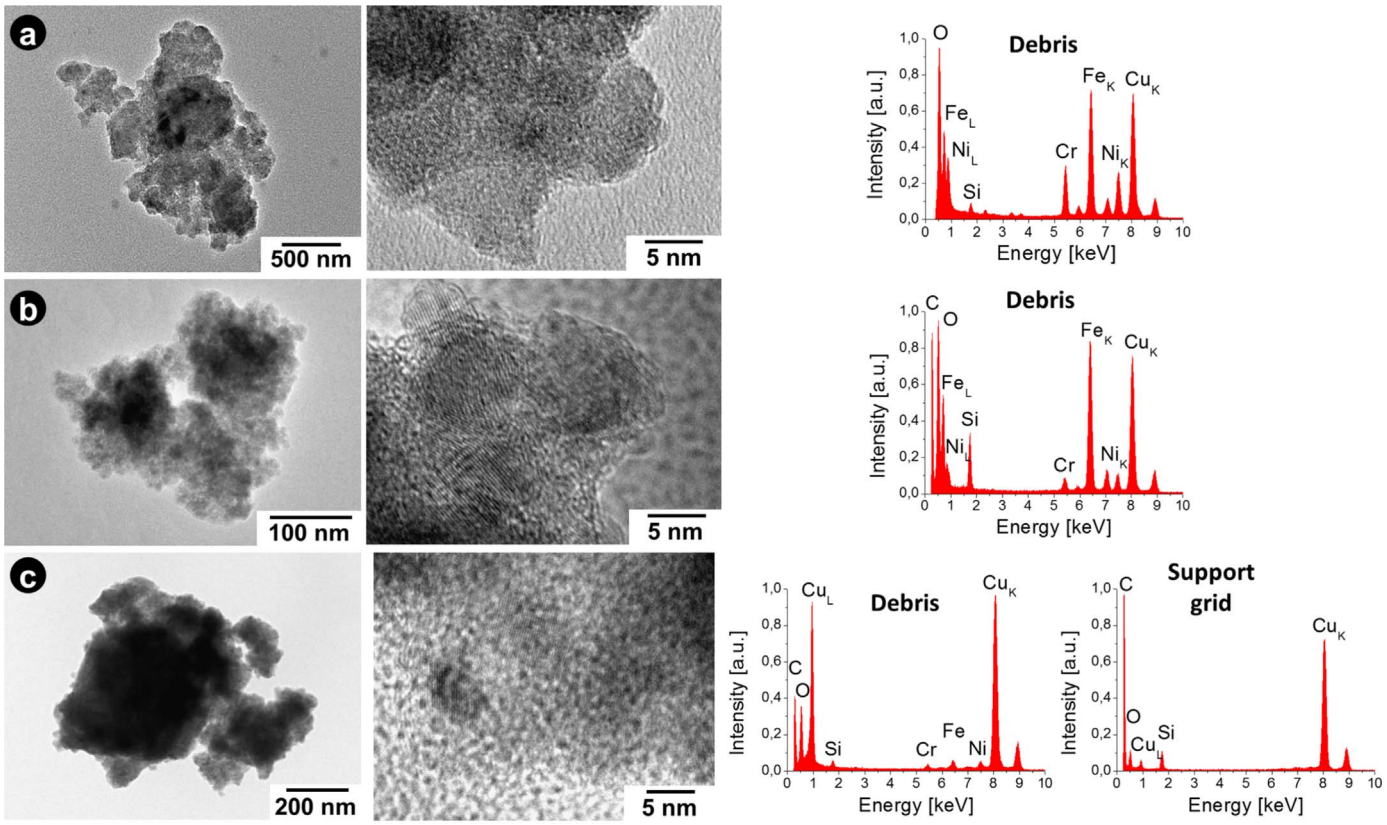

Fig. 11. TEM images and EDS spectra of debris corresponding to the different SGT/pad combinations: (a) I 800/AISI 304, (b) I 800/AISI 1060 and (c) I 800/Cu.

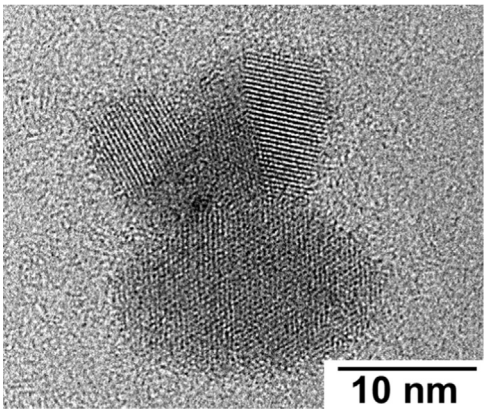

Fig. 12. HRTEM of nano-crystalline debris detached in fretting test of I 800/AISI 304.

obtained on the debris a strong Cu L peak is observed, which is a clear indication that it is was generated in an electron transparent region, and therefore confirms the presence of Cu in the debris. In all spectra, spurious Si peaks are observed that originate within the EDS detector.

The oxide phases in the debris were identified combining the information from the diffraction patterns with that of the EDS spectra. For the I 800/AISI 304 pair, the phases identified in the debris were NiO and a non-stoichiometric $(Ni,Fe)(Fe,Cr)_2O_4$ spinel. In addition, a weak ring of reflections is observed that corresponds to a modified $(Fe,Cr)_2O_3$ hematite where partial substitution of Fe by Cr takes place. In the case of the I 800/Cu and I 800/AISI 1060 pairs a single phase was identified in the debris. For the Cu pad an oxide with spinel structure was identified. EDS analysis indicated that the oxide was non-stoichiometric in composition, suggesting that it could be formulated as $(Cu,Ni)(Fe,Cr)_2O_4$ due to the presence of Ni, Fe and Cr in the debris. For the AISI 1060 pad, a hematite structure was identified that could be formulated as $(Fe,Cr)_2O_3$. In the latter EDS spectrum a small Ni peak was observed in the debris but reflections corresponding to crystalline structures with Ni were not identified in the ring patterns, presumably because they were too weak. In the different oxides that were identified, Fe^{2+}, Ni^{2+} and Cu^{2+} ions occupy tetrahedral sites while Fe^{3+} and Cr^{3+} ions occupy octahedral sites. The previously mentioned local variations of composition that were observed in the EDS spectra corresponded to length scales of a few tens of nanometers.

The presence of spinels with non-stoichiometric composition was detected in studies of corrosion in aqueous environment at temperatures near to service temperature in nuclear reactors in Incoloy 800 and AISI 304 L [25,26]. Also, in the development of magnetic materials, ferrites (Fe-spinels) are synthetized by mechanical milling of Fe_2O_3 and other bivalent metal oxides, MeO, resulting in $MeFe_2O_4$ type spinels [27]. On the other hand, $CuFe_2O_4$ has been obtained by mechanical milling at temperatures between 500 and 800 °C using CuO and Fe_2O_3 precursors [28]. Then, the presence of spinel structures in AISI 304 and Cu pads supports the hypothesis that debris generated during the fretting test that remain between the surfaces experiment a process similar to the mechanical milling as suggested in previous reports [16,17].

In addition to the mechanical milling process, an increase in the local temperature due to frictional power dissipation in fretting contact is expected. Recent finite element simulations that an oxide layer might significantly enhance the local temperature increase when its thermal conductivity is lower than that of the base material [29]. This could explain the presence of the complex cupro-spinel for I 800/Cu pair. Furthermore, in a recent study of the evolution of worn surfaces during fretting wear in Inconel 690TT [30], $NiCr_2O_4$ and Fe_2O_3 were found together with ultra-fine grains of NiO and Cr_2O_3 in the mixed zone near the tribologically transformed structure (TTS) layer.

Finally, for the I 800/AISI 1060 pair the crystalline structures observed in the debris were those typically found in corrosion studies of this type of steel. The presence of Ni in the debris can proceed only from

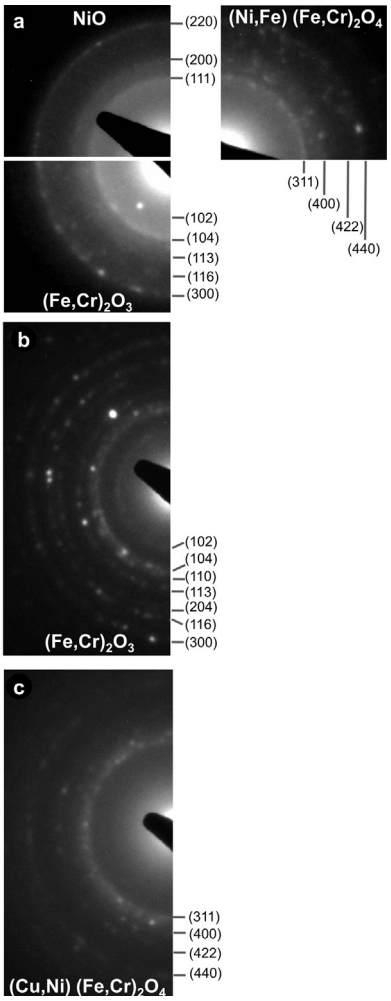

Fig. 13. Electron diffraction pattern and structure of debris for different pairs (a) I 800/AISI 304, (b) I 800/AISI 1060 and (c) I 800/Cu.

the SGT. However, it was not possible to identify the structures formed containing Ni in the EDP (Fig. 13). The only visible rings corresponded to a modified $(Fe,Cr)_2O_3$ hematite which present a partial substitution of Fe^{2+} for Cr^{2+}.

The prevalence of the adhesive or abrasive wear for the different pairs is influenced by the nature and characteristics of debris generated between the surfaces in contact.

For example, Kato [31] has reported a change in the mechanism of severe to mild wear in steels due to the presence of Fe_2O_3 particles with sizes between 30 nm and 500 nm that formed a compacted oxide layer, which prevented wear of the metal base. Therefore, the modified hematite $(Fe,Cr)_2O_3$ debris in the I 800/AISI 1060 pair together the high hardness of the pad is expected to prevent abrasive wear, leading to increased adhesive wear as shown in Fig. 4(b). Instead, the formation of high hardness layers of protective oxide Cr_2O_3 [32] at the beginning of the tests in the I 800/AISI 304 pair, together with the presence of NiO and $(Ni,Fe)(Fe,Cr)_2O_4$ spinel between the metallic surfaces hinders the protective effect of $(Fe,Cr)_2O_3$ and therefore the predominant mechanism is abrasive wear. Finally, in studies of wear of Cu alloys against steel a tendency of adhesive and delamination wear has been found [7,33], suggesting that adhesion is related with crystal structure and is strong in materials with similar crystal structure [7]. The prevalence of adhesive wear in I 800/Cu pair observed in the present work is therefore consistent with these reports.

In accordance with the results, the role of hardness of materials in contact is not as important for the fretting wear behaviour in Incoloy 800 as that of the debris microstructure. Similar results have been reported in other steels [34].

4. Conclusions

In the present study, the fretting wear behaviour of Incoloy 800 steam generator tubes against AISI 304, AISI 1060 and Cu solid cylindrical pads was studied.

It was found that adhesive wear was the predominant wear mechanism in the case of Cu and AISI 1060 pads while abrasive wear was predominant for the AISI 304 pad. In addition, high adherence between metal surface and a compacted debris layer was observed in SGTs for I 800/AISI 1060 and I 800/Cu. Therefore, the dominant wear mechanism was found to depend on the particular composition of the SGT/pad combination.

The Archard-based wear coefficient for the three pairs were very similar with an average value of $K = 8.4 \times 10^{-14}\ \mathrm{Pa}^{-1}$. However, EDS analysis demonstrated that an important fraction of material removed is deposited and adhered on SGT´s surface in the case of the AISI 1060 and Cu pads. This adhered volume is not computed as removed volume, and therefore influences the value of K.

From the point of view of the applications is important to mention that for the Cu and the AISI 1060 pads, the maximum pad scar depths differ considerably from that of the AISI 304 pad, in spite of the fact that wear coefficients are very similar. This suggests that K does not give a full picture of the damage development that might be useful for structural integrity analysis purposes.

The results obtained in the present work indicate that hardness falls short in being the main parameter controlling the wear process. Instead, the adhesion of a compacted debris layer, and therefore the specific wear mechanism, play a more significant role.

Debris detached for different pairs were larger particles with sizes around some hundreds nanometers which were formed by an agglomeration of crystallites with sizes of 5–20 nm. The analysis of debris crystalline structures indicates that for the I 800/AISI 304 pair the oxide particles consists of NiO, $(Fe,Cr)_2O_3$ and $(Ni,Fe)(Fe,Cr)_2O_4$, while for the I 800/Cu and I 800/AISI 1060 pairs, the formation of $(Cu,Ni)(Fe,Cr)_2O_4$ and $(Fe,Cr)_2O_3$ were observed, respectively. The kind of debris particles formed plays a significant role on the wear mechanism.

Acknowledgements

The assistance of Mr. Carlos Cotaro, Mr. Manuel Corte and Mrs. Paula Troyon with the SEM observations is gratefully acknowledged. Moreover, the support of Mr. Juan Pablo Balbiani with the fretting tests is gratefully acknowledged. We also acknowledge financial support from ANPCyT (PICT 0898–2011), CONICET and Universidad Nacional de Cuyo.

References

[1] IAEA, TECDOC-1668- Assessment and management of ageing of major nuclear power plant components important to safety: Steam generators, IAEA, Vienna, 2011.
[2] N.J. Fisher, A.B. Chow, M.K. Weckwerth, Experimental fretting-wear studies of steam generator materials, J. Press. Vessel- Technol. ASME 117 (1995) 312–320.
[3] R.B. Waterhouse, Fretting Corrosion, Pergamon Press, Oxford, 1972.
[4] J.M. Dobromirski, Variables of fretting process: are there 50 of them? in: M. Helmi Attia, R.B. Waterhouse (Eds.), ASTM STP 1159: Standardization of Fretting Fatigue Test Methods and Equipment, ASTM, Philadelphia, 1992, pp. 60–66.
[5] J. Li, Y. Lu, H. Zhang, L. Xin, Effect of grain size and hardness on fretting wear behavior of Inconel 600 alloys, Tribol. Int. 81 (2015) 215–222.
[6] K.G. Budinski, Effect of hardness differential on metal-to-metal fretting damage, Wear 301 (2013) 501–507.
[7] B. Bethune, R.B. Waterhouse, Adhesion of metal surfaces under fretting conditions II. Unlike metals in contact, Wear 12 (1968) 369–374.
[8] P. Blanchard, C. Colombie, V. Pellerin, S. Fayeulle, L. Vincent, Material effects in fretting wear: application to iron, titanium and aluminum alloys, Metall. Trans. A 22 (1991) 1535–1544.
[9] A. Iwabuchi, The role of oxide steel, Wear 151 (1991) 301–311.

[10] J.L. Xuan, H.S. Cheng, Microscopic wear debris generation and surface topography, in: D. Dowson, et al. (Ed.), Wear Particles: From the Cradle to the Grave, Elsevier, Amsterdam, 1992, pp. 247–256.
[11] J. Wei, S. Fouvry, Ph Kapsa, L. Vincent, Third body effects in fretting, in: D. Dowson, et al. (Ed.), The Third Body Concept, Elsevier, Amsterdam, 1996, pp. 45–53.
[12] J. Jiang, F.H. Stott, M.M. Stack, The role of triboparticulates in dry sliding wear, Tribol. Int. 31 (1998) 245–256.
[13] Special Metal Corporation, Publication Number SMC-046: INCOLOY® alloy 800, 2004.
[14] F.M. Guérout, N.J. Fisher, Steam generator fretting-wear damage: a summary of recent finding, J. Press. Vessel- Technol. ASME 121 (1995) 304–310.
[15] Y.H. Lee, H.K. Kim, H.D. Kim, C.Y. Park, I.S. Kim, A comparative study on the fretting wear of steam generator tubes in korean power plants, Wear 255 (2003) 1198–1208.
[16] S.R. Soria, A. Tolley, A. Yawny, A study of debris and wear damage resulting from fretting of Incoloy 800 steam generator tubes against AISI Type 304 stainless steel, Wear 368–369 (2016) 219–229.
[17] S.R. Soria, J.P. Balbiani, M. Bergant, A. Tolley, A. Yawny, Fretting damage in Incoloy® 800 tubes against different support materials, Procedia Mater. Sci. 9 (2015) 538–547.
[18] O. Vingsbo, S. Söderberg, On fretting maps, Wear 126 (1988) 131–147.
[19] ASTM G-204, Standard Test Method for Damage to Contacting Solid Surfaces under Fretting Conditions, ASTM Standard, Volume 03.02, 2013.
[20] S.R. Pearson, P.H. Shipway, Is the wear coefficient dependent upon slip amplitude in fretting? Vingsbo and Söderberg revisited, Wear 330–331 (2015) 93–102.
[21] E. Rabinowicz, The formation of spherical wear particles, Wear 42 (1977) 149–156.
[22] P.L. Hurricks, The occurrence of spherical particles in fretting wear, Wear 27 (1974) 319–328.
[23] T. Kayaba, A. Iwabuchi, Effect of hardness of hardened steels and the action of oxides on fretting wear, Wear 66 (1981) 27–41.
[24] J.D. Lemm, A.R. Warmuth, S.R. Pearson, P.H. Shipway, The influence of surface hardness on the fretting wear of steel pairs— Its role in debris retention in the contact, Tribol. Int. 81 (2015) 258–266.
[25] W. Kuang, E.H. Han, X. Wu, J. Rao, Microstructural characteristics of the oxide scale formed on 304 stainless steel in oxygenated high temperature water, Corros. Sci. 52 (2010) 3654–3660.
[26] B. Stellwag, The mechanics of oxide film formation on austenitic steel in high temperature water, Corros. Sci. 40 (1998) 337–370.
[27] B.D. Cullity, C.D. Graham, Introduction to Magnetic Materials, Willey, New Jersey, 2009.
[28] T.F. Marinca, I. Chicinaş, O. Isnard, Influence of the heat treatment conditions on the formation of $CuFe_2O_4$ from mechanical milled precursors oxides, J. Therm. Anal. Calorim. 110 (2012) 301.
[29] X. Jin, W. Sun, P.H. Shipway, The role of geometry changes and debris formation associated with wear on the temperature field in fretting contacts, Tribol. Int. 102 (2016) 392–406.
[30] L. Xin, B.B. Yang, Z.H. Wang, J. Li, Y.H. Lu, T. Shoji, Microstructural evolution of subsurface on Inconel 690TT alloy subjected to fretting wear at elevated temperature, Mat. Des. 104 (2016) 152–161.
[31] H. Kato, Severe–mild wear transition by supply of oxide particles on sliding surface, Wear 255 (2003) 426–429.
[32] H. Kitsunai, K. Hokkirigawa, N. Tsumaki, K. Kato, Transitions of microscopic wear mechanism for Cr_2O_3 ceramic coatings during repeated sliding observed in a scanning electron microscope tribosystem, Wear 151 (1991) 279.
[33] Z. Shi, Y. Sun, A. Bloyce, T. Bell, Unlubricated rolling-sliding wear mechanisms of complex aluminium bronze against steel, Wear 193 (1996) 235–241.
[34] R. Ramesh, R. Gnanamoorthy, Effect of hardness on fretting wear behaviour of structural steel, En 24, against bearing steel, En 31, Mater. Des. 28 (2007) 1447–1452.